# NEUTRAL AND CHARGED CURRENT DIS CROSS SECTIONS AT HIGH $Q^2$ FROM ZEUS AT HERA

J. GROSSE-KNETTER

*Particle & Nuclear Physics, Keble Road, Oxford, OX1 3RH, U.K.*
*E-mail: J.Grosse-Knetter1@physics.ox.ac.uk*

on behalf of the ZEUS Collaboration

Neutral and charged current deep inelastic scattering has been studied in $e^+p$ collisions at centre-of-mass energy of 300 GeV using the ZEUS detector at HERA. The data sample corresponds to a luminosity of $46.6\,\mathrm{pb}^{-1}$ collected in the period 1994-1997. Single and double differential cross sections are presented in the kinematic region $Q^2 > 400\,\mathrm{GeV}^2$ and good agreement with the Standard Model predictions is found, with the possible exception of two neutral current events with $Q^2 > 35000\,\mathrm{GeV}^2$.

## 1 Introduction

The deep inelastic scattering (DIS) of leptons by nucleons has proved to be an important tool both in the development of the current understanding of proton structure and in the determination of the form of the Standard Model (SM). Positron-proton collisions at HERA give access to DIS reactions at high momentum transfer squared, $Q^2$. At high $Q^2$ neutral current (NC) DIS is sensitive to the influence of the weak sector via exchange of $Z$ bosons, while charge current (CC) DIS is mediated by $W$ exchange only. In addition, NC and CC DIS is sensitive to parton distribution functions (PDFs), with the CC cross section focussing on particular combinations of quark and anti-quark PDFs.

Presented here is the measurement of NC and CC cross sections for $Q^2 > 400\,\mathrm{GeV}^2$ and their comparison to SM predictions. The measurements are based on $46.6\,\mathrm{pb}^{-1}$ of data collected by ZEUS from 1994 to 1997 during which HERA collided 27.5 GeV positrons with 820 GeV protons, for a centre-of-mass energy $\sqrt{s} = 300\,\mathrm{GeV}$.

## 2 Standard Model Cross Sections

The Born level cross section for the NC process $e^+p \to e^+X$ can be expressed as [1]:

$$\frac{d^2\sigma^{NC(e^+)}}{dxdQ^2} = \frac{2\pi\alpha^2}{xQ^4}\left[Y_+ F_2^{NC}(x,Q^2) - Y_- xF_3^{NC}(x,Q^2)\right]$$

where $x$ is the Bjorken scaling variable, $\alpha = 1/137$ the QED coupling constant and $Y_\pm = 1 \pm (1-y)^2$, with $y = Q^2/sx$. The longitudinal structure function $F_L^{NC}$ is expected to be below 1% and is thus neglected. The structure functions $F_2^{NC}$ and $xF_3^{NC}$ can be expressed in leading order QCD as sums over combinations of quark couplings and (anti-)quark momentum distributions.

The Born level cross section for the CC process $e^+p \to \bar{\nu}_e X$ can be expressed as:

$$\frac{d^2\sigma^{CC(e^+)}}{dxdQ^2} = \frac{G_F^2}{4\pi x}\left(\frac{M_W^2}{M_W^2+Q^2}\right)^2 \cdot \left[Y_+ F_2^{CC}(x,Q^2) - Y_- xF_3^{CC}(x,Q^2)\right]$$

where $M_W$ is the mass of the $W$-boson and $G_F$ the Fermi constant. The structure functions $F_2^{CC}$ and $xF_3^{CC}$ contain sums and differences of quark and anti-quark distributions [1]. The contribution of the longitudinal structure function $F_L^{CC}$ is again expected to be below 1% and neglected.

The primary uncertainty in the Born cross section is the uncertainty of the PDFs. ZEUS has estimated this uncertainty by extrapolating statistical and correlated systematic errors of fixed target data [2] in a NLO QCD fit. The result is a relative uncertainty of 6 to 8% in the predicted differential NC cross section $d\sigma/dQ^2$ and 9 to 17% in the CC cross section $d\sigma/dQ^2$.

## 3 Neutral Current Analysis

### 3.1 Event Selection

To select NC DIS ($e^+p \to e^+X$) events, a positron candidate is required with energy $E_e > 10\,\mathrm{GeV}$, with a matching track with momentum $P_{el}^{trk} > 5\,\mathrm{GeV}$ where appropriate, and with energy not associated to the candidate in an $\eta$-$\phi$-cone of radius 0.8 below 5 GeV. In addition, the $z$ coordinate of the vertex position must be between $-50$ and 100 cm, the difference between the sum of energies and longitudinal momenta of all particles $\delta = \sum(E-P_z)_i$ is required to be $38 < \delta < 65\,\mathrm{GeV}$, and background is removed by $y_e < 0.95$, $P_T < 4\sqrt{E_T}$, where $y_e$ is the $y$ variable as estimated from the positron candidate and $P_T$, $E_T$ are transverse momentum and energy, respectively. The kinematic range considered is $Q^2 > 400\,\mathrm{GeV}^2$.

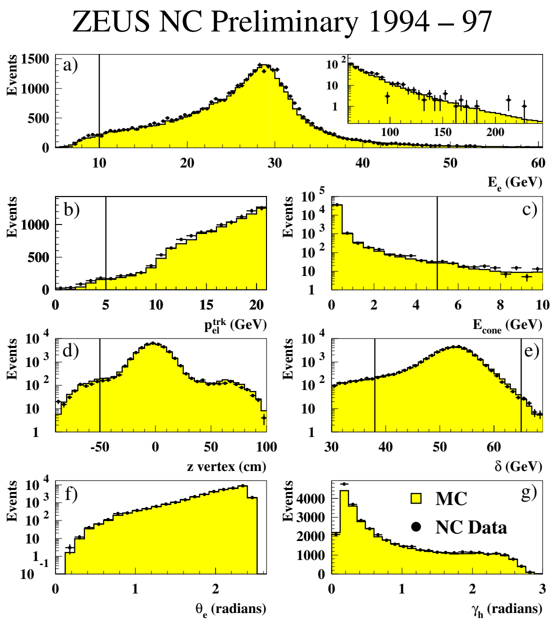


Figure 1: Comparison of NC DIS data (points) and Monte Carlo predictions (histograms) for (a) the positron energy $E_e$ (with the inset showing the high energy part); (b) the positron track momentum $P_{el}^{trk}$; (c) the energy $E_{\rm cone}$ not assigned to the positron in an $\eta$-$\phi$ cone of 0.8; (d) the $z$ position of the event vertex; (e) $\delta = \sum (E - P_z)_i$; (f) the positron angle $\theta_e$; (g) the hadronic angle $\gamma_h$. The lines indicate cuts applied to the quantities shown.

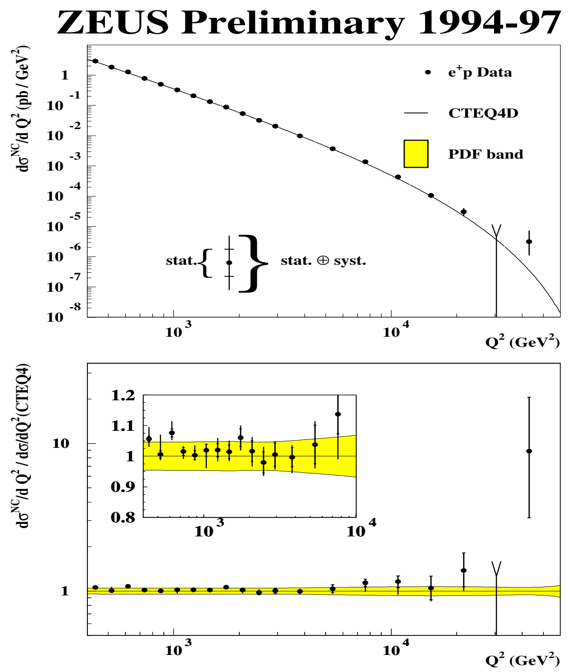


Figure 2: The NC DIS cross section $d\sigma/dQ^2$ for data (points) and the SM prediction using CTEQ4D PDFs (top) and the ratio (bottom) with the inset showing the ratio in enlarged linear horizontal scale. The inner error bars indicate the statistical errors. The shaded region is the uncertainty in the SM prediction due to the PDFs.

### *3.2 Simulation*

NC DIS events are simulated with radiative effects using the HERACLES [3] programme with the DJANGO [4] interface to hadronisation programmes. The latter is simulated using the colour-dipole model of ARIADNE [5] and, as a systematic check, the MEPS model of LEPTO [6]. The generated events are passed through a detector simulation subject to the same trigger requirements as the data and processed by the same reconstruction programmes.

A comparison between data and Monte Carlo expectations is shown in figure 1 for various event quantities. Good agreement is seen in all variables.

To estimate the background from photoproduction events are simulated using the Monte Carlo programme HERWIG [7], including a large sample of prompt photon events. The level of background is estimated to be 0.1% at $Q^2 = 400\,{\rm GeV}^2$ and to remain below 3% at high $Q^2$.

### *3.3 Results*

$Q^2$, $x$, and $y$ are measured with the double-angle method [8]. To calculate the Born level cross section $d\sigma/dQ^2$ integrated over the whole $y$ range, events are binned in reconstructed values of $Q^2$. The number of events in each bin is corrected for acceptance, migration, radiative and electroweak corrections and converted into a differential cross section. The result is plotted in figure 2 and compared to the SM prediction using parton momentum distributions from the CTEQ group [9]. All points agree with the SM predictions over several orders of magnitude within errors, with the exception of the highest bin $Q^2 > 36200\,{\rm GeV}^2$ which contains two events where 0.29 are expected. These events were reported previously [10], but no additional events are found in this high $Q^2$ bin with doubled luminosity.

The same procedure is used to obtain $d\sigma/dx$ and $d\sigma/dy$ as shown in figures 3 and 4 for different $Q^2$ thresholds. The SM predictions generally agree with the measured cross sections in the entire range of $x$ and $y$.

## 4 Charged Current Analysis

### *4.1 Event Selection*

To select CC DIS ($e^+p \rightarrow \bar{\nu}_e X$) events the scattered $\nu$ is tagged by requiring missing transverse momentum: $\not{P}_T > 10\,{\rm GeV}$. In addition, the absolute value of the $z$-coordinate of the vertex position must be below 50 cm. Background is removed by requiring $\not{P}_T/E_T > 0.4$ for $20 < \not{P}_T < 30\,{\rm GeV}$ (0.5 for $\not{P}_T < 20\,{\rm GeV}$), by identifying and rejecting NC DIS events, using cuts on timing,

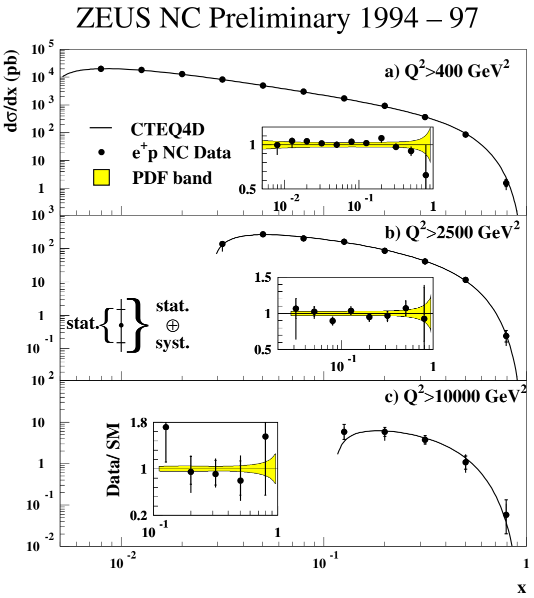


Figure 3: The NC DIS cross section $d\sigma/dx$ for data (points) and the SM prediction using CTEQ4D PDFs for (a) $Q^2 > 400\,\mathrm{GeV}^2$, (b) $Q^2 > 2500\,\mathrm{GeV}^2$, and (c) $Q^2 > 10000\,\mathrm{GeV}^2$. The insets show the ratio between data and prediction. The inner error bars indicate the statistical errors. The shaded region is the uncertainty in the SM prediction due to the PDFs.

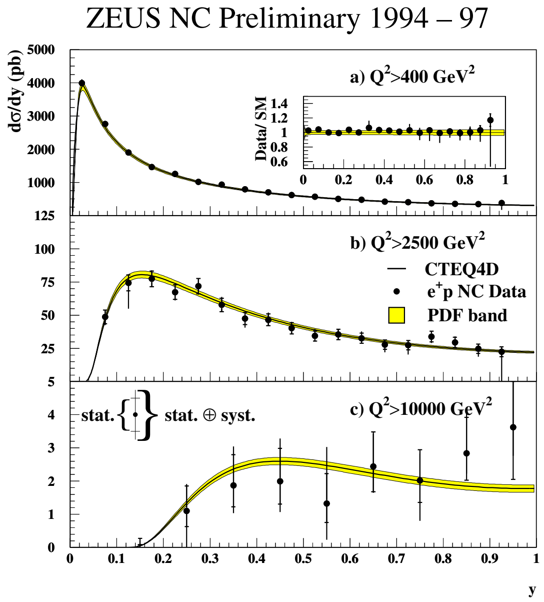


Figure 4: The NC DIS cross section $d\sigma/dy$ for data (points) and the SM prediction using CTEQ4D PDFs for (a) $Q^2 > 400\,\mathrm{GeV}^2$, (b) $Q^2 > 2500\,\mathrm{GeV}^2$, and (c) $Q^2 > 10000\,\mathrm{GeV}^2$. The insets in the top plot shows the ratio between data and prediction. The inner error bars indicate the statistical errors. The shaded region is the uncertainty in the SM prediction due to the PDFs.

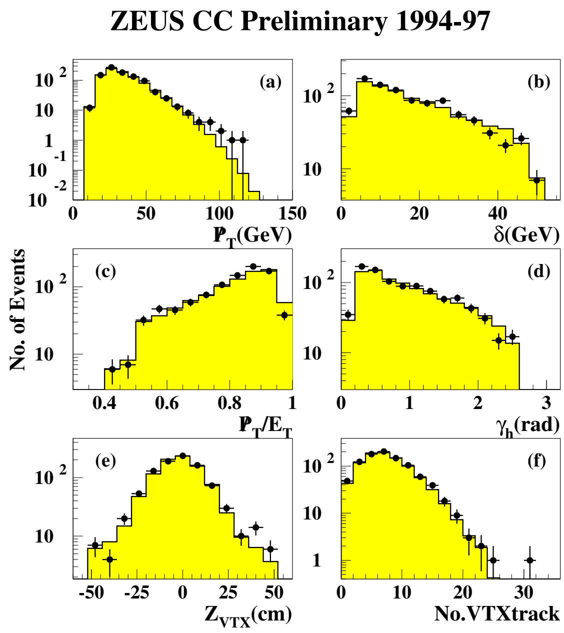


Figure 5: Comparison of CC DIS data (points) and Monte Carlo predictions (histograms) for (a) the net transverse momentum $\not{P}_T$; (b) $\delta = \sum(E - P_z)_i$; (c) $\not{P}_T/E_T$; (d) the hadronic angle $\gamma_h$; (e) the $z$ position of the event vertex; (f) the number of tracks assigned to the primary vertex.

via muon finding and a few other cuts. The kinematic range considered is $Q^2 > 400\,\mathrm{GeV}^2$ and $y < 0.9$, the cross sections being corrected for the latter.

### *4.2 Simulation*

CC DIS events are simulated with the HERACLES programme with the DJANGO interface to the hadronisation from ARIADNE and, as a systematic check, to that of the MEPS model of LEPTO. The generated events are again processed by the detector simulation, trigger, and reconstruction programmes as in the NC analysis.

A comparison between data and Monte Carlo expectations is shown in figure 5 for several quantities showing good agreement.

The HERWIG Monte Carlo programme is used again to estimate the background from photoproduction events. Background from NC DIS events is estimated with DJANGO, from $W$-production with EPVEC [11] and background coming from Bethe-Heitler with LPAIR [12] Monte Carlo samples. The level of background is typically 1% rising to at most 2.5% at low $Q^2$.

### *4.3 Results*

$Q^2$, $x$, and $y$ are measured with the Jacquet-Blondel method [13], applying corrections for the effect of energy

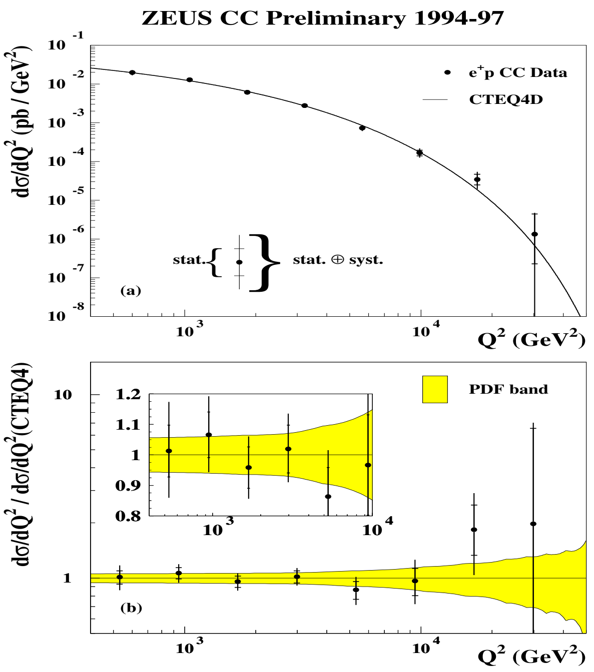


Figure 6: The CC DIS cross section $d\sigma/dQ^2$ for data (points) and the SM prediction using CTEQ4D PDFs (top) and the ratio (bottom) with the inset showing the ratio in enlarged linear horizontal scale. The inner error bars indicate the statistical errors. The shaded region is the uncertainty in the SM prediction due to the PDFs.

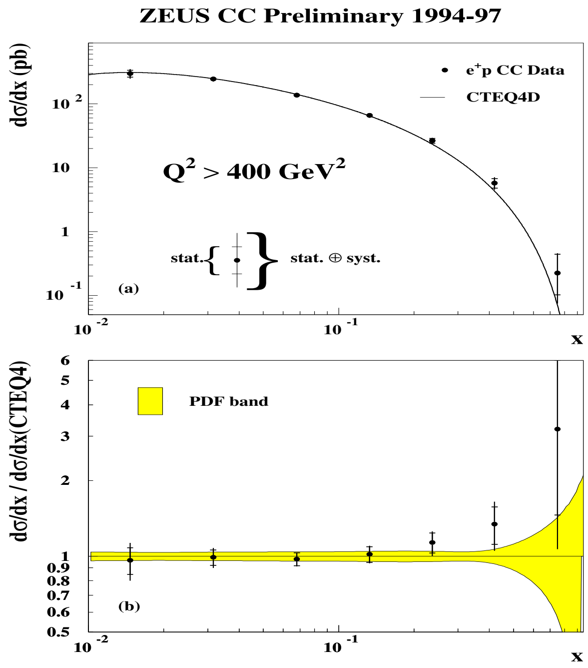


Figure 7: The NC DIS cross section $d\sigma/dx$ ($Q^2 > 400\,\mathrm{GeV}^2$) for data (points) and the SM prediction using CTEQ4D PDFs (top) and the ratio (bottom). The inner error bars indicate the statistical errors. The shaded region is the uncertainty in the SM prediction due to the PDFs.

lost in dead material. The Born level cross sections are determined with a bin-by-bin correction as described for the NC analysis above. The single differential cross sections $d\sigma/dQ^2$, $d\sigma/dx$, and $d\sigma/dy$ are shown in figures 6, 7, and 8, respectively. The expectations from the SM using parton momentum distributions from the CTEQ group is overlayed. A good agreement over most of the kinematic range is seen, though a tendency of the data to lie above the SM at high $Q^2$ and $x$ is observed.

The reduced double differential cross section, $\tilde{\sigma}$, which is defined from the measured cross section to be:

$$\tilde{\sigma} = \frac{d^2\sigma}{dx dQ^2}\left[\frac{G_F^2}{2\pi x}\left(\frac{M_W^2}{Q^2+M_W^2}\right)^2\right]^{-1} \quad (1)$$

is plotted as a function of $x$ for several fixed values of $Q^2$ in figure 9. At leading order $\tilde{\sigma}$ can be decomposed into contributions from the different PDFs as indicated in figure 9. As a result $\tilde{\sigma}$ is sensitive to the sea quark combination $\bar{u}+\bar{c}$ at low $x$ while the valence quark combination $d+s$ dominates at high $x$.

The $Q^2$ dependence of the CC cross section is determined by the $Q^2$ dependence of the PDFs and the propagator term $[M_W^2/(M_W^2+Q^2)]^2$. The value of $M_W$ is determined in a $\chi^2$ fit of the measured differential cross

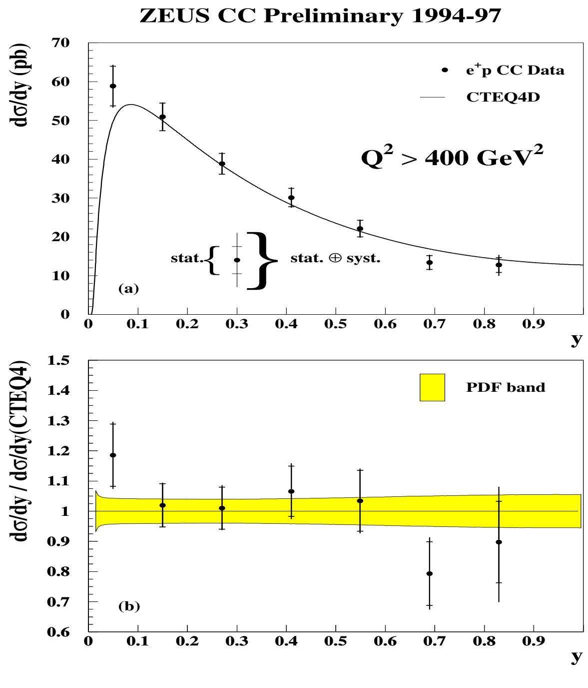


Figure 8: The NC DIS cross section $d\sigma/dy$ ($Q^2 > 400\,\mathrm{GeV}^2$) for data (points) and the SM prediction using CTEQ4D PDFs (top) and the ratio (bottom). The inner error bars indicate the statistical errors. The shaded region is the uncertainty in the SM prediction due to the PDFs.

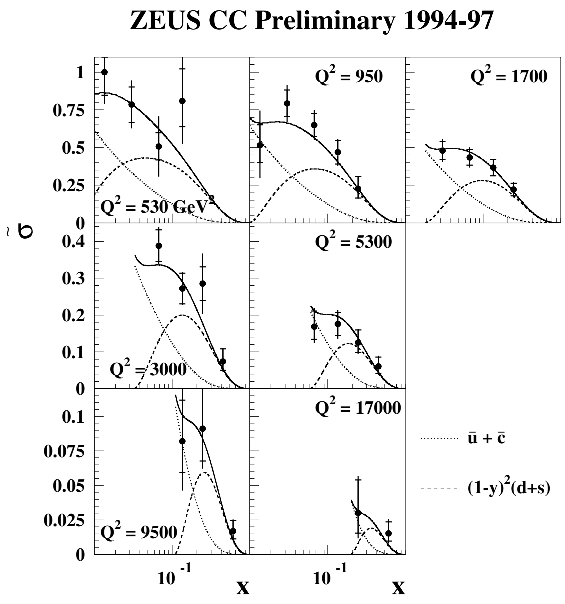


Figure 9: The CC DIS reduced cross section as defined in eq. (1) as a function of $x$ at fixed $Q^2$. The data are the solid points while the SM expectations are shown as the solid lines. The contributions of the PDF combinations $\bar{u}+\bar{c}$ and $(1-y)^2(d-s)$ evaluated at leading order are shown by the dotted and dashed lines respectively.

section $d\sigma(M_W)/dQ^2$, with $G_F$ fixed. The fit yields:

$$M_W = 78.6^{+2.5}_{-2.4}[\text{stat.}]^{+3.3}_{-3.0}[\text{syst.}]\,\text{GeV}.$$

This value is obtained using the CTEQ4D PDFs [9]. An additional uncertainty of $\pm 1.5\,\text{GeV}$ arises when $M_W$ is evaluated using a range of recent PDFs. This value of $M_W$ agrees with the current value of $M_W = 80.41 \pm 0.10\,\text{GeV}$ from the particle data group fit [14]. Since the propagator is space-like, the above result is complementary to a time-like mesurement of $M_W$ in $p\bar{p}$ or $e^+e^-$ annihilation and constitutes an important check of SM consistency.

## 5 Summary

The cross section for charged and neutral current deep inelastic scattering, $e^+p \to \bar{\nu}_e X$ and $e^+p \to e^+X$, has been measured in the kinematic region $Q^2 > 400\,\text{GeV}^2$ using $46.6\,\text{pb}^{-1}$ of data collected by the ZEUS detector during the period 1994 to 1997. The measured differential cross sections as functions of $Q^2$, $x$, and $y$ are well described by Standard Model predictions. The double differential charged current cross section $d^2\sigma/dxdQ^2$ has been determined for the first time at HERA and, again, the Standard Model gives a good description of the data. From the $Q^2$ dependence of the measured charged current cross section the mass of the exchanged $W$-boson has been determined to be $M_W = 78.6^{+2.5}_{-2.4}[\text{stat.}]^{+3.3}_{-3.0}[\text{syst.}]\,\text{GeV}$, in good agreement with direct measurements.

## Acknowledgements

The support by a Feodor Lynen fellowship of the Alexander von Humboldt foundation is highly appreciated.

## References

1. G. Ingelmann and R. Rückl, *Phys. Lett.* B **201**, 369 (1988);
   A.M. Cooper-Sakar, R. Devenish, and A. de Roeck, hep-ph/9712301 accepted by J. Mod. Phys. A.
2. L.W. Whitlow et al., *Phys. Lett.* B **282**, 475 (1992);
   BCDMS Collab., A.C. Benvenuti et al., *Phys. Lett.* B **223**, 485 (1989);
   BCDMS Collab., A.C. Benvenuti et al., *Phys. Lett.* B **237**, 592 (1990);
   NMC Collab., M. Arneodo et al., *Nucl. Phys.* B **483**, 3 (1997);
   CCFR Collab., P.Z. Qunitas et al., *Phys. Rev. Lett.* **71**, 1307 (1993).
3. HERACLES 4.4: A. Kwiatkowski, H. Spiesberger, and H.-J. Möhring, in: *Physics at HERA* **vol. 3**, 1194 (1991);
   A. Kwiatkowski, H. Spiesberger, and H.-J. Möhring, *Z. Phys.* C **50**, 165 (1991).
4. DJANGO 1: G. Schuler and H. Spiesberger, in: *Physics at HERA* **vol. 3**, 1419 (1991).
5. ARIADNE 4: L. Lönnblad, *Comput. Phys. Commun.* **71**, 15 (1992);
   L. Lönnblad, *Z. Phys.* C **65**, 285 (1995).
6. LEPTO 6.1: G. Ingelman, in: *Physics at HERA* **vol. 3**, 1366 (1991).
7. HERWIG 5.8: G. Marchesini et al., *Comput. Phys. Commun.* **67**, 465 (1992).
8. S. Bentvelsen, J. Engelen, and P. Krooijman, in: *Physics at HERA* **vol. 1**, 23 (1991);
   K.C. Hoeger, in: *Physics at HERA* **vol. 1**, 43 (1991).
9. H.L. Lai et al., *Phys. Rev.* D **55**, 1280 (1997).
10. ZEUS Collab., J. Breitweg et al., *Z. Phys.* C **74**, 207 (1997).
11. U. Baur, J.A.M. Vermaseren, D. Zeppenfeld, *Nucl. Phys.* B **375**, 3 (1992).
12. J.A.M. Vermaseren, *Nucl. Phys.* B **229**, 347 (1983).
13. F. Jacquet and A. Blondel, *Proc. of the study for an ep facility for Europe* **DESY 79-48**, 391 (1979).
14. C. Caso et al., Particle Data Group, *Euro. Phys. J.* C **3**, 1 (1998).